

Chemical Shift Encoding based Double Bonds Quantification in Triglycerides using Deep Image Prior

Chaoxing Huang,^{1,2} Ziqiang Yu,^{1,2} Zijian Gao,^{1,2} Qiuyi Shen^{1,2}, Queenie Chan³,

Vincent Wai-Sun Wong⁴, Winnie Chiu-Wing Chu^{1,2}, Weitian Chen^{1,2}

1. Department of Imaging and Interventional Radiology, The Chinese University of Hong Kong, Hong Kong SAR
2. CUHK Lab of AI in Radiology (CLAIR), The Chinese University of Hong Kong, Hong Kong SAR
3. Philips Healthcare, Hong Kong SAR
4. Department of Medicine & Therapeutic, The Chinese University of Hong Kong, Hong Kong SAR

Word count: around 2500 words

Numbers of Figures and Tables: 6

Running Title: DIP for Mapping Double Bonds

Address correspondence to:

Weitian Chen

Room 15, Sir Yue Kong Pao Centre for Cancer

Prince of Wales Hospital Shatin, NT

Hong Kong

(852)-3505-1036

Email: wtchen@cuhk.edu.hk

Abstract

This study evaluated a deep learning-based method using Deep Image Prior (DIP) to quantify triglyceride double bonds from chemical-shift encoded multi-echo gradient echo images without network training. We employed a cost function based on signal constraints to iteratively update the neural network on a single dataset. The method was validated using phantom experiments and in vivo scans. Results showed close alignment between measured and reference double bond values, with phantom experiments yielding a Pearson correlation coefficient of 0.96 ($p = .0005$). In vivo results demonstrated good agreement in subcutaneous fat. We conclude that Deep Image Prior shows feasibility for quantifying double bonds and fatty acid content from chemical-shift encoded multi-echo MRI.

Keywords: Deep Learning, Number of Double Bonds, Triglyceride, MRI

1. INTRODUCTION

Chemical-shift encoding–based water–fat separation methods have been developed to quantify fat content (1,2). Recently, there has been growing interest in quantifying the fatty acid composition of fat due to its potential in evaluating metabolic disorders and inflammatory conditions (3). Previous studies indicate that the key to quantifying the fatty acid composition lies in determining the number of double bonds in triglycerides (4,5). Optimization algorithms have been proposed to quantify this variable using chemical-shift encoded multi-echo methods (4-6).

In recent years, there is strong interest in applying deep neural networks in quantitative MRI (qMRI) for tasks such as image reconstruction and parameter mapping. Quantitative MRI collects data in higher dimensions than the conventional anatomical imaging. Deep learning shows promising performance in handling high-dimensional data (7). However, most deep learning-based methods require a substantial amount of data to train the neural network. For many medical imaging tasks, it is challenging or even impractical to collect sufficient amount of training data. Deep image prior (DIP) method (8) has been proposed as an unsupervised learning method to address ill-posed

inverse problems using deep network without requiring any training data. The original DIP approach was found promising in image denoising and restoration tasks (8-10). The recent work demonstrated the potential of DIP in medical imaging tasks where training data is difficult to acquire, including PET image reconstruction and restoration (11-13) and MR image reconstruction (14-17).

One challenge for quantifying the number of double bonds in triglycerides is that it is highly susceptible to signal perturbations, making it an ill-posed problem. Deep learning approaches were previously reported promising in quantitative MRI in the presence of signal perturbations (18,19). However, training a deep neural network requires a sufficient amount of data and the data available for quantifying fatty acid is scarce in the community. The properties of DIP make it a proper choice to address these issues in quantifying the numbers of double bonds in triglycerides via neural networks. In this work, we investigated DIP for mapping the number of double bonds in triglycerides from multi-echo MRI. We demonstrated the feasibility and advantages using both phantom and in vivo experiments.

2. METHODS

2.1 Signal model

The multi-peak multi-echo signal with water and fat contents at echo time t can be expressed as (4) :

$$S(W, F, ndb, nmldb, \phi; t) = (W + Ff \sum_{m=1}^M \alpha_m(ndb, nmldb) e^{i\omega_m t}) e^{i\phi t} \quad (1)$$

where W, F are water and fat signal, respectively; ϕ is a complex map with the real and imaginary component representing the field map and R2* map, respectively; $f = \frac{1}{\sum_{m=1}^M \alpha_m}$ is the

normalization factor; α_m is the amplitude of the m th fat peak and is the function of the number of double bonds (ndb) and the number of methylene-interrupted double bonds ($nmidb$); and ω_m is the known chemical shift of the m th fat peak. We adopt the eight-peak fat model in (4), which is also referred as the “free model”. More details of the free model can be found in Table 1 in (4).

2.2 Network fitting

We first recap the basic concept of deep image prior and present its extension to the mapping of numbers of double bonds in triglyceride. The DIP method is unsupervised and interprets the output of a deep network as a parametrization of an image (8). Originally, the deep network $f_\theta(\cdot)$ with network weight θ takes a randomized map \mathbf{z} as input and map it to a denoised image with the same size. Given a noisy image I , the denoised image I^* can be obtained by minimizing the following equation:

$$\theta^* = \underset{\theta}{\operatorname{argmin}} \|I - f_\theta(\mathbf{z})\|, I^* = f_{\theta^*}(\mathbf{z}) \quad (2)$$

The network is enforced to reconstruct the noisy image I through iterations and early stopping is applied so that the output tensor is a denoised image rather than the noisy one. The DIP is based on an assumption that the structure of an autoencoder- like architecture already captures the main image statistics, which is independent of learning. Those statistics priors are associated with low-level image features, and it is the must-need information to recover an image with high fidelity from a degraded one. Intuitively, the clean image with high fidelity can emerge during the process of reconstructing the noisy image by using those image statistics.

As for quantifying the parametric maps in our task, the network is defined as a parametric map generator and the optimization can be defined as follows:

$$\tilde{\theta} = \underset{\theta}{\operatorname{argmin}} \frac{1}{PE} \sum_{p=1}^P \sum_{e=1}^E (L(S(f_\theta(\mathbf{z}), t_e)_p, y_{e_p})) \quad \square$$

$$A = f_{\theta}(\mathbf{z}), \quad (3)$$

where A is the estimated parametric map; e is the index of the echo and y_e stands for the acquired signal under the corresponding time of echo; p is the index of the pixels in an image; and L is the cost function and L1 norm is chosen as the cost function.

The network takes the randomized map as input and the network parameters are updated iteratively following the optimization in equation (3). The result arrives once the loss function is converged.

The network has five outputs, including W , Ff , ϕ , ndb and $nmidb$. The complex images W , Ff , ϕ have two output channels, one for the real part and the other for the imaginary part. The ndb and $nmidb$ outputs have one channel. We group the fat signal term F and the normalization factor term f into one term as we empirically find it more stable to fit the network. The fat signal can be recovered once ndb and $nmidb$ are obtained as they can be used to compute the normalization factor. The fat fraction (FF) is defined as $Real(\frac{F}{W+F})$. Sigmoid function is placed at the channel of ndb to limit its range from 0 to 6 as this is the typical range of the numbers of double bonds (5). We adopt a UNet like architecture for the deep network (20).

2.3 Data Acquisition

The in vivo study received approval from the institutional review board. We employed the multi-echo gradient echo sequence protocol described in (21) to acquire the images. Scans were performed using a Philips Elition 3T MRI scanner (Philips Healthcare, Best, the Netherlands). A 32-channel head coil and a 32-channel cardiac coil were used as the receiver for phantom and abdominal imaging, respectively. A total of 14 echoes were acquired with the following parameter settings: $TE_1/\Delta TE = 1.20/0.7$ ms, TR = 10 ms, Flip angle = 20 degrees, matrix size = 160×120 ,

$FOV = 400 \times 300mm$, and slice thickness = 6 mm. Seven slices were scanned. All datasets were collected in axial plane. For in vivo scan, the dataset of each slice was acquired in a single breath hold of 17 seconds.

2.4 Implementation details

The experiments were conducted in a computing environment running Windows 11 with Python 3.7. All experiments were implemented using PyTorch 1.9 (22). The computational tasks were performed on a system equipped with an RTX 4090 GPU and an i9-13900 CPU. For comparative analysis, we also implemented the algorithm described in (6) to quantify number of double bonds by fitting the data to the eight-peak free model. In the subsequent discussion, we refer to this method as least square fitting (LSF), as it is based on the LSF method of water-fat separation (2). All images were cropped to ensure the samples occupied the majority part of the image. The Adadelta optimizer (23) was employed, and the learning rate was set to $5e-2$. The fitting was conducted for 180,000 iterations and it took around an hour to complete.

2.5 Phantom experiment

To validate the measured ndb values of different vegetable oils by comparing them to the reference values previously published (5,24), we prepared 50mL tubes of various kinds of pure vegetable oil. These tubes were immersed in water bath in our phantom. In addition to the pure oil phantoms, we also used corn oil and created a representative water-fat phantom with a fat fraction of approximately 60% to evaluate the algorithm's ability to quantify the number of double bonds in the presence of mixed water and fat. The creation of the water-fat phantom followed the protocol outlined in (25). The agar solution was prepared by heating and mixing distilled water, agar powder, sodium dodecyl sulfate, and sodium benzoate (all sourced from Sigma Aldrich, St.

Louis, MO, USA). The agar and oil solutions were blended, stirred, heated, and subsequently cooled to form the water-fat phantom.

The analysis of the results was performed within regions of interest (ROIs). Circular ROIs were placed at the center of each tube. The mean and the standard deviation of all pixel values within the ROIs of all slices were calculated.

2.6 In-vivo experiment

We performed an in-vivo abdomen scan on two healthy volunteers. The ROIs were chosen on the area of subcutaneous fat. The mean value within the ROIs of all the slices was compared with previously published reference values (5,24). Note the protocol was initially used for liver scan and a shimming box was placed on right part of the liver parenchyma, therefore we only use left part of the images for fitting.

3. Results

Table 1 shows the fitted result compared with the reference values of both the DIP and the LSF method.

Figure 1 shows the maps of the number of double bonds and the number of methylene-interrupted double bonds from the pure oil phantoms. Note the measured values are close to the expected values, and all the tubes show an FF to nearly 100%.

Figure 2 illustrates the regression plot depicting the correlation between the measured values and the reference values of *ndb* and *nmidb* for both the DIP method and the LSF method. The plot reveals a strong correlation, and the regression lines closely align with the reference plot of $y=x$. For the LSF method, the Pearson correlation coefficient between the measured values and the reference values is 0.98 ($p = 8.89e-5$) for *ndb* and 0.98($p = 9.34e-5$) for *nmidb*. The regression analysis yields a slope of 1.04 and an intercept of -0.29 for *ndb* and a slope of 0.98 and an intercept of -0.04 for *nmidb*. Similarly, the DIP method exhibits a reasonable correlation performance, with a Pearson correlation coefficient of 0.96 ($p = .0005$) for *ndb* and 0.96 ($p = .0006$) for *nmidb*. The regression analysis of DIP yields a slope of 0.92 and an intercept of 0.35 for *ndb* and a slope of 0.90 and an intercept of 0.20 for *nmidb* .

Figure 3 shows the results from the phantom with mixed water and fat made from corn oil. Note the measured values are consistent between the pure oil phantom and the phantom with mixed oil and water when using the DIP-based method, with values of 4.50 and 4.43, respectively. The measured *ndb* and *nmidb* in the pure oil phantom is 4.50 and 1.88, respectively. And those in the phantom with mixed oil is 4.43 and 1.83, respectively. In contrast, the LSF method exhibits a large error in measuring the *ndb* and *nmidb* in the phantom with mixed water and fat, likely due to the fact that the LSF method requires exceedingly high fat fraction to provide sufficient SNR for reliable quantification of the number of double bonds. The robustness of DIP method can also be appreciated from its closer fat fraction (FF) result (62.76%) to the reference value (60%). In contrast, the LSF method yields FF with a larger deviation (66.70%).

Figure 4 shows the in-vivo measured results obtained from both methods of two typical slices. Note the published reference value of *ndb* and *nmidb* of fat in the subcutaneous region are 2.88 and 0.70, respectively (5). The measured values of both healthy volunteers are shown in Table 2, indicating a reasonable alignment of the measured values and the reference values.

By using the DIP approach, the measured *ndb* in our study are 1.62 ± 0.51 and 2.91 ± 1.22 at the liver and the subcutaneous region, respectively. In contrast, the measured *ndb* using the LSF approach are 3.91 ± 3.68 and 3.06 ± 1.53 at the liver and the subcutaneous region, respectively, which are considerably higher than the reference values, likely due to its susceptibility to noise. Note that a considerable number of pixels in the liver parenchyma has *ndb* value beyond the normal range from 0 to 6 when using the LSF method.

4. DISCUSSION

We demonstrated the feasibility of using the DIP-based method to measure the numbers of double bonds in triglycerides from chemical shift-encoded multi-echo gradient echo images. The results obtained from pure oil phantoms and subcutaneous fat show agreement between the measured values and the reference values. We observed that the DIP method demonstrated a superior performance compared to LSF method in the mixed water-fat phantom. We attribute the better performance to the denoising ability of the DIP method. The convolutional neural network architecture itself is assumed to have the ability to capture implicit prior of the image, filter out noise and generate the main content of the image with high fidelity. In the original DIP method for denoising application, the network is enforced to reconstruct a noisy image while the image with reduced noise emerges after early-stop of iterations. In our work, the DIP network is enforced to reconstruct the gradient echo images from the parametric maps. It is likely inherent denoising

effect in the signal domain contribute to the fitting of the parametric maps, and thus improves robustness to estimate *ndb* and *nmidb* map compared to the LSF method when the fat signal is reduced.

It is important to note that the DIP-based method for fitting the numbers of double bonds is unsupervised and does not need pretraining the neural network. Self-supervised learning methods have been proposed for parametric MRI, which do not require ground truth for training but still require a substantial number of unlabeled images as the training data (26,27). In contrast, DIP only trains the network on a single dataset and the training itself is the inference. It may have potential significance in other learning-based qMRI mapping tasks, in which it is challenging to acquire training data.

While our initial validation of using DIP to fit the numbers of double bonds is promising, this work has limitations. The network needs to be retrained each time for a new mapping task, which was also pointed out in the original DIP work. This increases the computation cost of inference. It is also important to conduct more in vivo studies on patients with various fat fractions to understand the feasibility of the DIP approach in clinical imaging.

5. CONCLUSION

We demonstrated the feasibility of using DIP to fit the number of double bonds in triglycerides from chemical shift-encoded multi-echo gradient echo MRI. Further studies are needed to validate its use in clinical environments.

ACKNOWLEDGMENT

This study was supported by a grant from the Research Grants Council of the Hong Kong SAR (Project GRF 14213322), and a grant from the Innovation and Technology Commission of the Hong Kong SAR (Project No .MRP/046/20x).

Footnote

Conflicts of Interest: All authors have completed the ICMJE uniform disclosure form. The authors have no conflicts of interest to declare.

Ethical Statement:

A: The authors are accountable for all aspects of the work in ensuring that questions related to the accuracy or integrity of any part of the work are appropriately investigated and resolved.

B: The authors are accountable for all aspects of the work in ensuring that questions related to the accuracy or integrity of any part of the work are appropriately investigated and resolved. The trial was conducted in accordance with the Declaration of Helsinki (as revised in 2013). The study was approved by institutional/regional/national ethics/committee/ethics board of CUHK and informed consent was taken from all individual participants.

Reference

- [1] Dixon WT. Simple proton spectroscopic imaging. *Radiology*. 1984;153(1):189-94.
- [2] Reeder SB, McKenzie CA, Pineda AR, Yu H, Shimakawa A, Brau AC, et al. Water–fat separation with IDEAL gradient-echo imaging. *Journal of Magnetic Resonance Imaging: An Official Journal of the International Society for Magnetic Resonance in Medicine*. 2007;25(3):644-52.

- [3] Reddy JK, Sambasiva Rao M. Lipid metabolism and liver inflammation. II. Fatty liver disease and fatty acid oxidation. *American Journal of Physiology-Gastrointestinal and Liver Physiology*. 2006;290(5):G852-G8.
- [4] Trinh L, Peterson P, Leander P, Brorson H, Månsson S. In vivo comparison of MRI-based and MRS-based quantification of adipose tissue fatty acid composition against gas chromatography. *Magnetic Resonance in Medicine*. 2020;84(5):2484-94.
- [5] Bydder M, Girard O, Hamilton G. Mapping the double bonds in triglycerides. *Magnetic resonance imaging*. 2011;29(8):1041-6.
- [6] Peterson P, Månsson S. Simultaneous quantification of fat content and fatty acid composition using MR imaging. *Magnetic resonance in medicine*. 2013;69(3):688-97.
- [7] Zhu Y, Cheng J, Cui Z-X, Zhu Q, Ying L, Liang D. Physics-Driven Deep Learning Methods for Fast Quantitative Magnetic Resonance Imaging: Performance improvements through integration with deep neural networks. *IEEE Signal Processing Magazine*. 2023;40(2):116-28.
- [8] Ulyanov D, Vedaldi A, Lempitsky V, editors. Deep image prior. *Proceedings of the IEEE conference on computer vision and pattern recognition*; 2018.
- [9] Liu J, Sun Y, Xu X, Kamilov US, editors. Image restoration using total variation regularized deep image prior. *ICASSP 2019-2019 IEEE International Conference on Acoustics, Speech and Signal Processing (ICASSP)*; 2019: Ieee.
- [10] Liu Y, Pan J, Ren J, Su Z, editors. Learning deep priors for image dehazing. *Proceedings of the IEEE/CVF international conference on computer vision*; 2019.
- [11] Hashimoto F, Ote K, Onishi Y. PET image reconstruction incorporating deep image prior and a forward projection model. *IEEE Transactions on Radiation and Plasma Medical Sciences*. 2022;6(8):841-6.

- [12] Hashimoto F, Ote K, Onishi Y. PET image reconstruction incorporating deep image prior and a forward projection model. *IEEE Transactions on Radiation and Plasma Medical Sciences*. 2022;6(8):841-846.
- [13] Kaplan S, Zhu Y-M. Full-dose PET image estimation from low-dose PET image using deep learning: a pilot study. *Journal of digital imaging*. 2019;32(5):773-8.
- [14] Lin Y-C, Huang H-M. Denoising of multi b-value diffusion-weighted MR images using deep image prior. *Physics in Medicine & Biology*. 2020;65(10):105003.
- [15] Darestani MZ, Heckel R. Accelerated MRI with un-trained neural networks. *IEEE Transactions on Computational Imaging*. 2021;7:724-33.
- [16] Yoo J, Jin KH, Gupta H, Yerly J, Stuber M, Unser M. Time-dependent deep image prior for dynamic MRI. *IEEE Transactions on Medical Imaging*. 2021;40(12):3337-48.
- [17] Yazdanpanah AP, Afacan O, Warfield SK, editors. Non-learning based deep parallel MRI reconstruction (NLDpMRI). *Medical Imaging 2019: Image Processing*; 2019: SPIE.
- [18] Huang C, Wong VW-S, Chan Q, Chu WC-W, Chen W. An uncertainty aided framework for learning based liver T₁ ρ mapping and analysis. *Physics in Medicine & Biology*. 2023;68(21):215019.
- [19] Shih SF, Kafali SG, Calkins KL, Wu HH. Uncertainty-aware physics-driven deep learning network for free-breathing liver fat and R2* quantification using self-gated stack-of-radial MRI. *Magnetic Resonance in Medicine*. 2023;89(4):1567-85.
- [20] Buda M, Saha A, Mazurowski MA. Association of genomic subtypes of lower-grade gliomas with shape features automatically extracted by a deep learning algorithm. *Computers in biology and medicine*. 2019;109:218-25.

- [21] Paisant A, Boulic A, Bardou-Jacquet E, Bannier E, D'assignies G, Lainé F, et al. Assessment of liver iron overload by 3 T MRI. *Abdominal Radiology*. 2017;42:1713-20.
- [22] Paszke A, Gross S, Massa F, Lerer A, Bradbury J, Chanan G, et al. Pytorch: An imperative style, high-performance deep learning library. *Advances in neural information processing systems*. 2019;32.
- [23] Zeiler MD. Adadelata: an adaptive learning rate method. *arXiv preprint arXiv:12125701*. 2012.
- [24] Trinh L. Quantification of Fatty Acid Composition Using MRI: Comparison of Accuracy at 1.5, 3 and 7 T. 2013.
- [25] Hines CD, Yu H, Shimakawa A, McKenzie CA, Brittain JH, Reeder SB. T1 independent, T2* corrected MRI with accurate spectral modeling for quantification of fat: validation in a fat-water-SPIO phantom. *Journal of Magnetic Resonance Imaging: An Official Journal of the International Society for Magnetic Resonance in Medicine*. 2009;30(5):1215-22.
- [26] Liu F, Kijowski R, El Fakhri G, Feng L. Magnetic resonance parameter mapping using model-guided self-supervised deep learning. *Magnetic resonance in medicine*. 2021;85(6):3211-26.
- [27] Huang C, Qian Y, Yu SC-H, Hou J, Jiang B, Chan Q, et al. Uncertainty-aware self-supervised neural network for liver T1 ρ mapping with relaxation constraint. *Physics in Medicine & Biology*. 2022;67(22):225019.

Figures

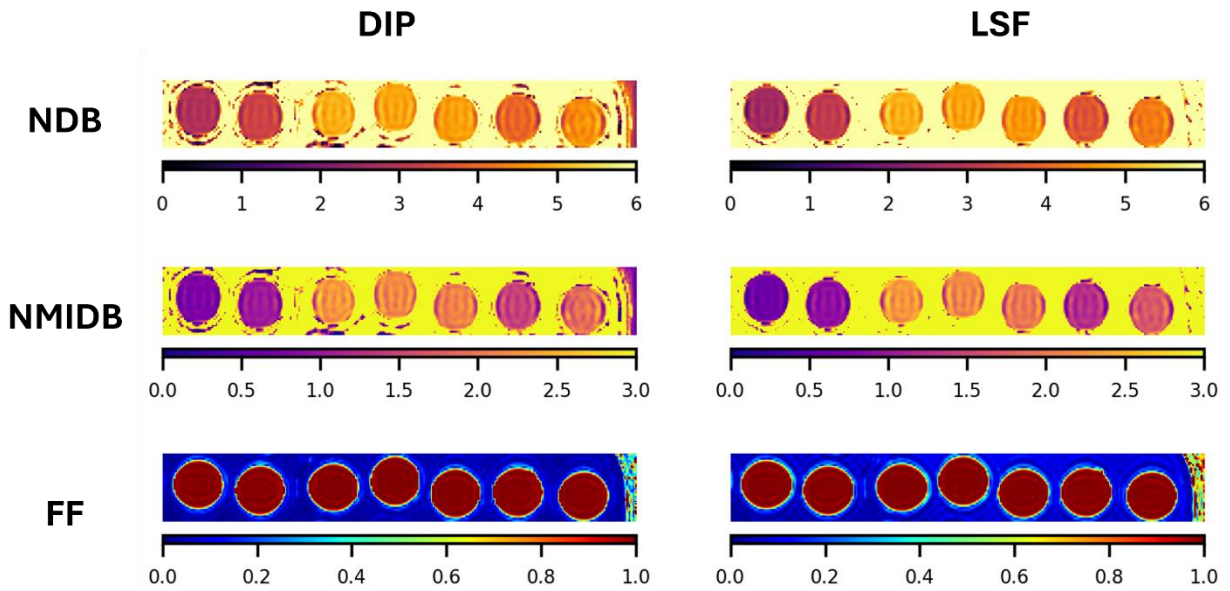


Figure 1: The measured *ndb* and *nmidb* using both the DIP and LSF method. From the left to the right in each plot are maps from Olive, Peanut, Safflower, Walnut, Grapeseed, Canola, and Corn oil, respectively.

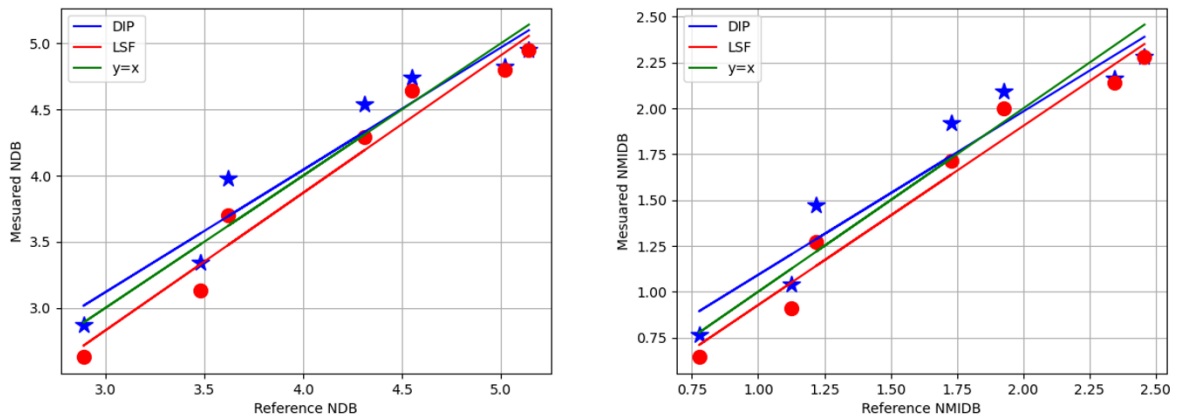


Figure 2: Regression plot of the measured *ndb* and *nmidb* values and the reference values

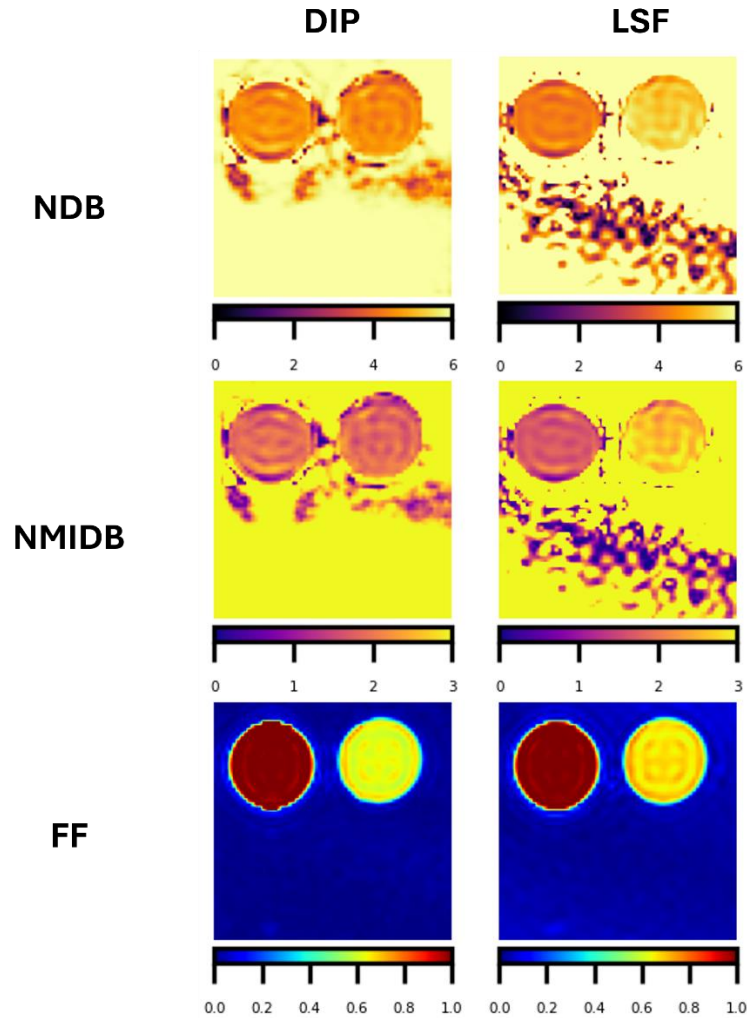
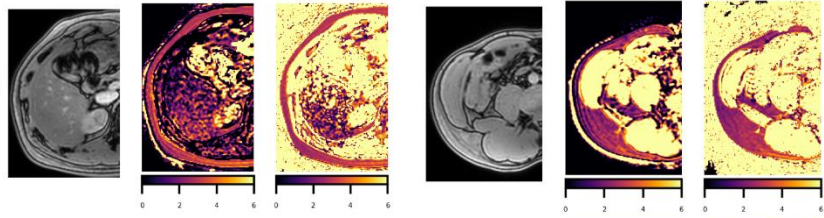


Figure 3: The measured number of double bonds from the pure oil phantom and the phantom with mixed water and oil. From the left to the right are the phantom with pure oil and the phantom with mixed oil and water (FF = 60%). The DIP method yields consistent measurement in two phantoms (pure oil ndb = 4.50, mixed phantom ndb = 4.43, pure oil nmidb = 1.88, mixed oil phantom ndb = 1.83). The LSF method shows inconsistent measurement for two phantoms (pure oil ndb = 4.32, mixed phantom ndb = 5.27, pure oil nmidb = 1.72, mixed phantom nmidb = 2.58), respectively.

Anatomy & NDB



NMIDB

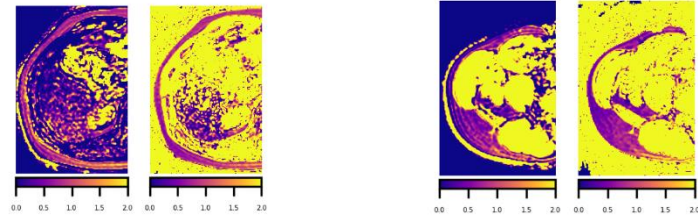


Figure 4: In-vivo mapping of *ndb* and *nmidb* using DIP and LSF.

Tables

NDB			
Oil category	DIP	LSF	Reference
Safflower	4.95±0.24	4.95±0.23	5.14
Walnut	4.82±0.23	4.80±0.25	5.02
Grapeseed	4.74±0.22	4.64±0.25	4.55
Canola	3.98±0.24	3.70±0.24	3.62
Corn	4.54±0.30	4.29±0.24	4.31
Olive	2.87±0.19	2.63±0.23	2.89
Peanut	3.34±0.20	3.13±0.23	3.48
NMIDB			
Oil category	DIP	LSF	Reference
Safflower	2.28±0.12	2.27±0.10	2.34
Walnut	2.16±0.13	2.14±0.16	2.32
Grapeseed	2.08±0.11	2.00±0.14	2.3
Canola	1.47±0.09	1.27±0.11	1.14
Corn	1.92±0.17	1.71±0.15	1.75
Olive	0.77±0.12	0.64±.13	0.35
Peanut	1.04±0.13	0.91±0.23	1.01

Table 1: The measured values of the *ndb* and *nmidb* of different types of oils using DIP and LSF method from the pure oil phantoms. The reference value of the grapeseed oil is from reference [25] while the rest are from reference [5].

	DIP	LSF
Volunteer 1 ndb	2.91±1.22	3.06 ± 1.53
Volunteer 1 nmidb	0.79 ± 0.23	0.87 ± 0.20
Volunteer 2 ndb	2.55 ± 0.49	2.64±0.47
Volunteer 2 nmidb	0.60 ±0.13	0.65±0.15

Table 2: The measured ndb and nmidb of the two healthy volunteers for subcutaneous fat.